Shear Jamming and Fragility of Suspensions in a Continuum Model with Elastic Constraints

Giulio G. Giusteri*
Dipartimento di Matematica, Università degli Studi di Padova, Via Trieste 63, 35121 Padova, Italy

Ryohei Seto†
Wenzhou Institute, University of Chinese Academy of Sciences, Wenzhou, Zhejiang 325001, China; Oujiang Laboratory (Zhejiang Lab for Regenerative Medicine, Vision and Brain Health), Wenzhou, Zhejiang 325001, China; and The Graduate School of Information Science, University of Hyogo, Kobe, Hyogo 650-0047, Japan

(Received 1 February 2021; accepted 20 August 2021; published 20 September 2021)

Under an applied traction, highly concentrated suspensions of solid particles in fluids can turn from a state in which they flow to a state in which they counteract the traction as an elastic solid: a shear-jammed state. Remarkably, the suspension can turn back to the flowing state simply by inverting the traction. A tensorial model is presented and tested in paradigmatic cases. We show that, to reproduce the phenomenology of shear jamming in generic geometries, it is necessary to link this effect to the elastic response supported by the suspension microstructure rather than to a divergence of the viscosity.

DOI: 10.1103/PhysRevLett.127.138001

The rheology of highly concentrated suspensions of solid particles dispersed in a viscous fluid features a number of surprising phenomena [1–3], among which shear jamming raises important questions for its interpretation and challenges for its mathematical modeling. If the concentration of particles is not very high, the suspension presents a fluidlike behavior. At high concentrations, one can instead observe a sudden solidification that occurs after some strain in a shear deformation, whence the name of shear jamming.

Under those conditions, the constant stress applied to the suspension is balanced by the elastic response of the solidified medium, arguably sustained by the network of contacts developed among the solid particles during the initial flow [4–7]. The shear-jammed material is in a fragile state: if the applied stress is removed no motion arises, but if we reverse the stress, pushing in a sufficiently different direction, the suspension flows again and stops only once a certain strain is accumulated. This history-dependent or protocol-dependent rheological response marks a key difference from states of isotropic jamming, in which the suspension is so concentrated as to be unable to flow, irrespective of the direction of the applied forces.

We present a constitutive model that is able to reproduce the phenomenology of shear jamming and fragility. We base its construction on the understanding that shear jamming corresponds to the onset of an elastic response, related to geometric constraints at the microscale, rather than to a boost in dissipative phenomena, as implied by models containing a divergence of the viscosity. We devised an effective and yet mathematically simple model, that features a small number of parameters easily linked to experimental measurements.

We define a tensorial model at the outset, without going through the process of designing a scalar model—typically tailored to a restricted set of motions—and then extending it. In this way, our model is readily applicable to flows in general two- and three-dimensional geometries, both boundary- and pressure-driven ones.

In the past decade, a few models to describe the physics of dense suspensions have been proposed, with a focus on capturing discontinuous shear thickening and rationalizing the role of frictional contacts between the solid particles [8–14]. A common feature of such models is the attempt at building a direct link between the emergent behavior and the microstructure of the fluid, as characterized by the analysis of data coming from detailed simulations at the microscale level [15,16]. In relation to shear jamming, these models are not readily applicable to the macroscale simulation of this phenomenon, as they identify the jammed state with a divergence of the viscosity [17] rather than the onset of elastic responses, so that mathematical singularities appear in the equations. On the other hand, we can find important results in the construction of continuum models that focus on the macroscale dynamics [18] and utilize a two-material approach, by following the coupled evolution of homogenized fluid and solid phases. Such models are quite effective in reproducing certain observations but feature several parameters that require calibration and involve a set of equations with considerable complexity.

Our model is intended to capture the suspension behavior at a rather large scale, when a single-fluid model is appropriate. We do not take explicitly into account particle migration phenomena [19–21] and rate dependence of the viscosity or stress-induced solidification [17,22,23]. These

can be incorporated for specific applications as extensions of the model but are not essential to reproduce shear jamming. In fact, we stress that it is possible to give a very good qualitative description of shear jamming assuming a constant viscosity, by associating jamming with the appearance of elasticity.

The phenomenon of shear jamming can be viewed as the emergence of solidity due to the evolution of the suspension microstructure. The activation of frictional contacts between the particles leads to the presence of percolating stable formations that span macroscopic portions of the system [5,6,24–26]. This microscopic nonlocality of the internal interactions marks the transition from a regime in which momentum is transferred slowly and diffusively (viscous fluid) to a regime in which momentum travels fast and elastically across the system (jammed solid). When the elastic response is very stiff, one can even approach the macroscopic nonlocality represented by rigid-body motions.

Another important aspect brought at the forefront by shear jamming is the material memory. We obviously observe a long-lasting memory of what would be the relaxed configuration in the jammed solid regime, but there is also a memory in the microstructure evolution that governs the type and amount of deformation possible within the fluid regime, in which no persistent elasticity is detected [16,27]. Both these aspects need to be captured in an effective continuum theory and we propose to use tensorial models for all of them. As we shall see, the kinematic descriptors of the system that are useful for our purposes are the velocity field and its gradient, to capture the viscous dissipation, and a tensorial measure of the strain induced on the material by the motion. The latter quantity keeps track of the microstructural deformation and, by limiting its evolution with unilateral constraints in the appropriate space of tensors, we can capture the transition between the fluid regime and the solid one, meanwhile preserving the characteristic reversibility represented by the fragility of the shear-jammed state.

The tensorial model.—A crucial role in shear jamming is played by the history of the deformation, as it induces some organization of the suspension microstructure, eventually responsible for the solidlike behavior. Alongside the evolution equation for the velocity field $\boldsymbol{u}$ of a fluid with mass density ρ,

$$\rho\left(\frac{\partial \boldsymbol{u}}{\partial t}+(\boldsymbol{u}\cdot\nabla)\boldsymbol{u}\right)=\mathrm{div}\mathbf{T}, \tag{1}$$

driven by the Cauchy stress tensor $\mathbf{T}$, we consider the evolution equation for the deformation gradient tensor $\mathbf{F}$ [see [28], Chap. 3, Sec. 3.2] in spatial coordinates:

$$\frac{\partial \mathbf{F}}{\partial t}+(\boldsymbol{u}\cdot\nabla)\mathbf{F}=(\nabla\boldsymbol{u})\mathbf{F}. \tag{2}$$

Equation (2) is an exact kinematic relation between the velocity and the displacement of fluid elements and does not contain any constitutive assumption.

From $\mathbf{F}$ we define $\mathbf{B}\equiv\mathbf{F}\mathbf{F}^{\mathsf{T}}$ and $\mathbf{L}\equiv\frac{1}{2}\log\mathbf{B}$, where log denotes the matrix logarithm. This is well defined because the left Cauchy-Green tensor $\mathbf{B}$ is symmetric and positive definite for any physical motion. These kinematic quantities track the local strain by factoring out rigid rotations, which should not affect the elastic response. The tensor $\mathbf{L}$ is the spatial counterpart of the Hencky strain and a generalization of the scalar strain measured in simple shear flows. Several advantages of its use are discussed in Ref. [29].

An important feature of $\mathbf{L}$ is that it is traceless whenever $\det\mathbf{B}=1$. This is always the case for us, because we assume incompressibility of the material, namely $\mathrm{div}\,\boldsymbol{u}=0$ at all times. We write the stress tensor as a pressure term plus the traceless extra stress $\mathbf{S}$, so that $\mathbf{T}=-p\mathbf{I}+\mathbf{S}$. The extra stress is the sum of a viscous dissipation plus an elastic response. The dissipative term takes the form $2\eta\mathbf{D}$, wherein the effective viscosity η of the suspension multiplies the symmetric part of the velocity gradient $\mathbf{D}\equiv(\nabla\boldsymbol{u}+\nabla\boldsymbol{u}^{\mathsf{T}})/2$.

Regarding the elastic contribution to the stress, we assume that there exists a predetermined subset $\mathcal{N}$ in the space $\mathcal{S}$ of local strains (symmetric and traceless tensors) corresponding to states in which the material is *elastically neutral*. It means that, at each point $\boldsymbol{x}$ and instant t, if $\mathbf{L}(\boldsymbol{x},t)$ is in $\mathcal{N}$ there is no elastic response. This assumption is motivated by the observation that there is a regime in which particle contacts contribute to the effective viscosity but do not store elastic energy and the macroscopic response is purely viscous. In our model, the elastic response will be proportional to a suitable measure of how far $\mathbf{L}(\boldsymbol{x},t)$ is from $\mathcal{N}$. The overall isotropy of the suspension suggests to take $\mathcal{N}$ to be a ball centered at the null tensor, namely $\mathcal{N}\equiv\{\mathbf{M}\in\mathcal{S}:\|\mathbf{M}\|\le r\}$ where, for any arbitrary tensor $\mathbf{M}$, we set $\|\mathbf{M}\|^2\equiv\mathrm{tr}(\mathbf{M}^{\mathsf{T}}\mathbf{M})/2$ and $r>0$ is a dimensionless material parameter that indicates how much the suspension needs to be sheared to achieve a jammed microstructure (and identifies the radius of $\mathcal{N}$). The value of r would typically be a decreasing function of the volume fraction of solid particles. When $r=0$ the suspension is an elastic solid, as under isotropic jamming.

Because $\mathcal{N}$ is a closed convex subset of $\mathcal{S}$, a projection operator $\Pi:\mathcal{S}\to\mathcal{N}$ is well defined and, for any $\mathbf{M}\in\mathcal{S}$, the tensor $\Pi(\mathbf{M})$ is the element of $\mathcal{N}$ closest to $\mathbf{M}$. Such a projection can be easily expressed as

$$\Pi(\mathbf{M})\equiv\begin{cases}\mathbf{M} & \text{if } \|\mathbf{M}\|\le r,\\ r\mathbf{M}/\|\mathbf{M}\| & \text{if } \|\mathbf{M}\|>r.\end{cases} \tag{3}$$

To reflect the fact that an elastic response is activated whenever the logarithmic measure of strain $\mathbf{L}$ leaves the neutral subset $\mathcal{N}$, we assume an extra stress of the form

$$\mathbf{S} = 2\eta\mathbf{D} + 2\kappa(\mathbf{L} - \Pi(\mathbf{L})), \tag{4}$$

where the material parameter $\kappa > 0$ represents an elastic stiffness. This is a "soft" way of constraining the strain (as opposed to keeping it always within $\mathcal{N}$) that is able to better reproduce some details of the elastic effects observed in the proximity of jamming [7]. With the present model, the strain of the jammed material tends to remain close to the boundary of $\mathcal{N}$ if the applied stress is driving it outward. Conversely, the suspension can flow again as soon as the stress drives $\mathbf{L}$ toward the interior of $\mathcal{N}$. In this way we can capture both shear jamming and the fragility of the jammed state.

The tensor $\Pi(\mathbf{L})$ corresponds to a conformation tensor. It describes a microstructure that closely follows the strain $\mathbf{L}$ up to the boundary of $\mathcal{N}$, where shear jamming prevents further microstructural deformations. The inclusion of additional dissipative phenomena, which may appear at the onset of jamming, can be achieved by letting η depend on a parameter such as $\lambda \equiv \|\mathbf{L} - \Pi(\mathbf{L})\|$.

Planar extensional flows.—We highlight the basic features of the model in an idealized case, for which analytical computations can be carried out. Under the deformation associated with planar extensional flows, the current position of a particle that occupies the place (x_0, y_0) at time 0 is given by $\boldsymbol{\varphi}(x_0, y_0, t) = (x_0 e^{\varepsilon(t)}, y_0 e^{-\varepsilon(t)})$ and its spatial inverse is $\boldsymbol{\varphi}^{-1}(x, y, t) = (x e^{-\varepsilon(t)}, y e^{\varepsilon(t)})$, where $\varepsilon(t)$ is an arbitrary function of time and measures the strain of the material. We immediately obtain $\mathbf{F} = \mathrm{diag}(e^{\varepsilon(t)}, e^{-\varepsilon(t)})$ and consequently $\mathbf{B} = \mathrm{diag}(e^{2\varepsilon(t)}, e^{-2\varepsilon(t)})$. In this case, the computation of the matrix logarithm is straightforward and yields $\mathbf{L} = \mathrm{diag}(\varepsilon(t), -\varepsilon(t))$.

The velocity is $\boldsymbol{u}(t) = (\dot{\varepsilon}(t)x, -\dot{\varepsilon}(t)y)$ and the symmetric part of the velocity gradient, the usual measure of the rate of deformation, is

$$\mathbf{D} = \begin{pmatrix} \dot{\varepsilon}(t) & 0 \\ 0 & -\dot{\varepsilon}(t) \end{pmatrix} = \frac{\partial \mathbf{L}}{\partial t}. \tag{5}$$

We stress that the second identity in (5) is not valid for a generic flow (it does not hold, e.g., in simple shear); when vorticity is present, rotation affects the deformation history in a nontrivial way, and $\mathbf{D}$ and $\mathbf{L}$ cannot remain aligned. This fact corresponds to the well-known presence of normal stress differences in simple shear flows of viscoelastic fluids.

We consider the extensional flow in a cross channel with hyperbolic boundaries that allow for a perfect slip of the fluid [Fig. 1(a)]. A pressure difference applied to inlets and outlets of the channel generates normal tractions $\tau\boldsymbol{n}$ at outlets and $-\tau\boldsymbol{n}$ at inlets, where $\boldsymbol{n}$ is the unit outer normal to the boundary. In a slow-velocity regime, the linearized flow equations give the pressure field $p(x, y, t) = \rho\ddot{\varepsilon}(t)(y^2 - x^2)/2$. The balance of stress at $(x, y) = (l, 0)$ yields the following equation:

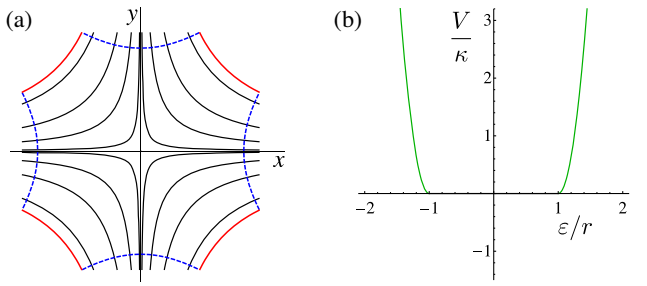

FIG. 1. We can imagine planar extension in a cross channel (a), with hyperbolic boundaries (red solid lines) that allow for perfect slip, to which we apply a pressure difference between the top or bottom inlet and right or left outlet (blue dashed lines). The linearized equations for the proposed model reduce in this case to the scalar ordinary differential equation (6) for the strain function ε. Considering the elastic force in Eq. (6), we see that it corresponds to that of a damped oscillator with (b) an elastic potential energy V featuring a flat region for $\varepsilon \in [-r, r]$.

$$\frac{\rho l^2}{2}\ddot{\varepsilon} + 2\eta\dot{\varepsilon} - \tau = \begin{cases} -2\kappa[\varepsilon + r] & \text{if } \varepsilon < -r, \\ +0 & \text{if } -r \le \varepsilon \le r, \\ -2\kappa[\varepsilon - r] & \text{if } \varepsilon > r, \end{cases} \tag{6}$$

where the dimensionless parameter r denotes, as above, the radius of the neutral subset $\mathcal{N}$. The derivation of Eq. (6) is reported in the Supplemental Material [30], Sec. A.

This is a scalar ordinary differential equation for the strain $\varepsilon(t)$, equivalent to that of a damped oscillator with elastic potential energy that features a flat region for $\varepsilon \in [-r, r]$ and parabolic branches outside that interval [Fig. 1(b)]. This entails transitions between a viscous fluid behavior, for $\varepsilon \in [-r, r]$ when there is no elastic force, and that of a viscoelastic solid when elastic forces are activated.

Clogging and unclogging.—Let us now consider how the model performs in simulating a paradigmatic pressure-driven flow through a contraction. In this planar flow, the maximum width of the channel (Fig. 3) equals the contraction length ℓ, while the contraction width is $\ell/4$. The total length of the domain is 4ℓ and we assume a uniform unit depth. Periodic boundary conditions for $\boldsymbol{u}$ and $\mathbf{F}$ are imposed at the left and right boundary of the domain, while no-slip conditions are assumed on the top and bottom walls. The pressure is not periodic: a pressure difference Δp between the right and left openings is driving the flow.

We introduce a dimensionless form of the evolution equations by defining a reference pressure difference P and taking the channel width ℓ as reference length. A reference timescale is $t_0 \equiv \ell\sqrt{\rho/P}$, leading to $\tilde{t} = t/t_0$. From these, we set the Reynolds number Re and the dimensionless elasticity constant $\tilde{\kappa}$ according to

$$\mathrm{Re} \equiv \frac{\ell\sqrt{\rho P}}{\eta} \quad \text{and} \quad \tilde{\kappa} \equiv \frac{2\kappa\ell}{\eta}\sqrt{\frac{\rho}{P}},$$

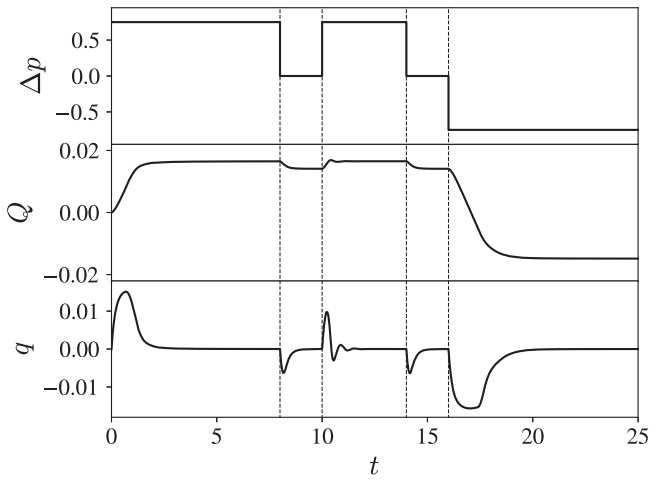

FIG. 2. The present model can reproduce the features of shear jamming in a complex flow through a contraction. We varied the pressure difference $\Delta p(t)$ imposed between the left and the right opening and measured the flow rate $q(t)$ through a cross section of the channel and its time integral $Q(t) = \int_0^t q(s)ds$. Parameters in the simulation: channel width equals the contraction length ℓ, while the contraction width is $\ell/4$; $\mathrm{Re} = 20\sqrt{0.75} \approx 17$, $\tilde{\kappa} = 100/\sqrt{0.75} \approx 116$, and $r = 1.5/\sqrt{2}$.

and so that the dimensionless flow equation reads

$$\mathrm{Re}\left(\frac{\partial \tilde{\boldsymbol{u}}}{\partial \tilde{t}} + (\tilde{\boldsymbol{u}} \cdot \nabla)\tilde{\boldsymbol{u}}\right) = -\nabla \tilde{p} + \nabla^2 \tilde{\boldsymbol{u}} + \tilde{\kappa}\,\mathrm{div}(\mathbf{L} - \Pi(\mathbf{L})). \tag{7}$$

In what follows we consider all quantities as dimensionless but drop the tildes for simplicity.

At startup, Δp is set positive, the flow accelerates and the flow rate reaches a maximum at about $t = 1$ (Fig. 2). The deformation induced by the flow gives rise to shear-jammed domains that grow from the boundaries toward the center of the contraction [Fig. 3(b)]. This activates an elastic response within the material that hinders the flow. The pressure drop in the clogged state ($t = 8$) is sustained by jammed regions with a characteristic sawtooth shape [Fig. 3(c)]. The intensity of the elastic response in each region depends on the local pressure drop. When we remove the pressure difference, from $t = 8$ to $t = 10$ (and again from $t = 14$ to $t = 16$), the stored elastic energy is completely released with a small recoil and then the flow stops (Fig. 2). Nevertheless, the microstructure remembers to be close to shear jamming and when the pressure difference is turned on again ($t = 10$) only a small fluid displacement is produced because we assist to a rapid reactivation of the elastic response inside the contraction.

On the other hand, when Δp is reversed to a negative value, the flow lasts for a longer time and the fluid displaced through the contraction before shear jamming sets in again is about twice as much as that displaced in the

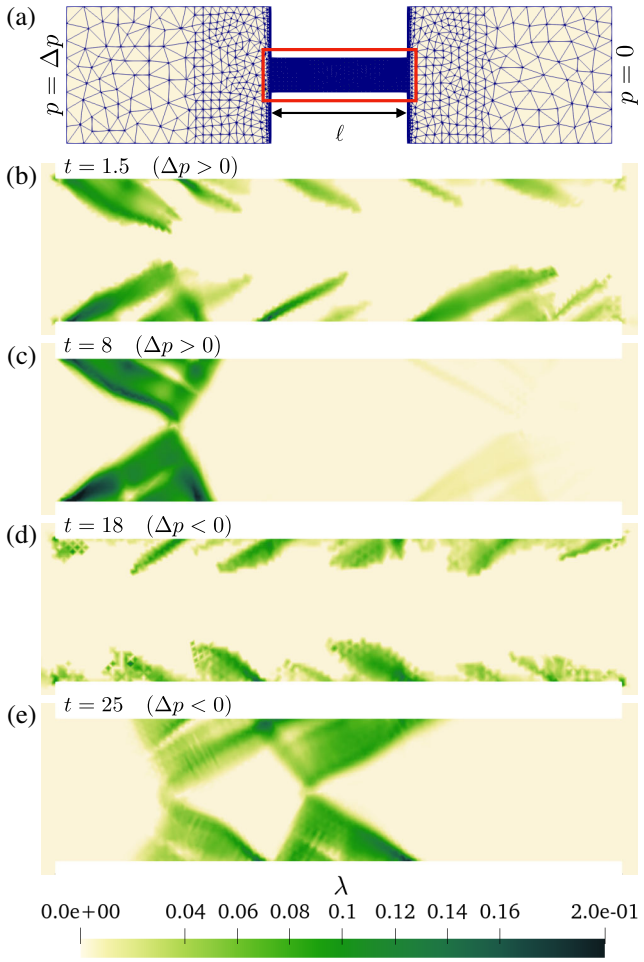

FIG. 3. (a) The entire domain is shown with the discretized mesh. (b)–(e) The clogging of the channel is due to the presence, within the contraction to which images are restricted, of shear-jammed domains. These are characterized by a nonvanishing elastic response measured by the parameter $\lambda \equiv \|\mathbf{L} - \Pi(\mathbf{L})\|$. From panels (b) and (d) we can see that the jammed domains nucleate and grow from the contraction boundaries, where the strain grows faster. There is a clear difference between the shear-jammed state (c) achieved at $t = 8$ with a positive Δp, which pushes rightward, and (e) the one obtained at $t = 25$ after reorganization with a negative Δp, which pushes leftward. In particular, the sawtooth shape of the jammed regions is reflected.

first part of the experiment (Fig. 2). The shear-jammed domains, where the elastic response is active, are destroyed and rebuilt with a different spatial distribution by the reverse flow [Fig. 3(d)]. The elastic stress at $t = 25$ [Fig. 3(e)] sustains two subsequent pressure drops of about $\Delta p/2$, thus showing two pairs of equally stresses jammed domains. At $t = 8$, the total pressure drop is almost entirely sustained by the jammed domains on the left, while only a slight elastic response is visible on the right side of the contraction [Fig. 3(c)]. By mimicking randomness in the suspension microstructure [22] with spatial fluctuations of the initial deformation gradient, we obtained a more

realistic nucleation of the shear-jammed regions. This random seed is at the origin of the asymmetry between the jamming process for positive or negative Δp. Details on the dependence of simulation results on meshing and material parameters, together with movies of the time evolution of pressure, flow, and elastic response are presented in the Supplemental Material [30].

Conclusions.—We have shown how the knowledge about a complex collective phenomenon, acquired by means of experiments and simulations, can be transferred into a rather simple model of the macroscale physics that we observe. By relating shear jamming to the activation of an elastic response and not to a divergence of the viscosity, we developed a tensorial model able to reproduce the qualitative features of shear jamming.

Such a model can be applied to generic flows and geometries in both two and three dimensions, because it rests on physical considerations that are not peculiar to a specific experimental setup. It becomes particularly useful to simulate the flow of suspensions in applications, where the focus is on the emergent collective physics and not on its microscopic origins.

Notably, we simulated a material able to switch, in a reversible way, between a fluidlike and a solidlike behavior. This feature, essential to capture shear jamming, can suggest effective ways to deal also with yielding phenomena. While we kept the model as simple as possible, many extensions can be implemented to reproduce a rate-dependent behavior.

G. G. G. acknowledges the support of the Italian National Group of Mathematical Physics (GNFM-INdAM) through the funding scheme GNFM Young Researchers' Projects 2020. R. S. acknowledges the support from the Wenzhou Institute, University of Chinese Academy of Sciences, under Grant No. WIUCASQ D2020002.

*giulio.giusteri@math.unipd.it
†seto@ucas.ac.cn

[1] É. Guazzelli and O. Pouliquen, J. Fluid Mech. **852**, P1 (2018).
[2] J. F. Morris, Annu. Rev. Fluid Mech. **52**, 121 (2020).
[3] M. M. Denn and J. F. Morris, Annu. Rev. Chem. Biomol. Eng. **5**, 203 (2014).
[4] M. E. Cates, J. P. Wittmer, J.-P. Bouchaud, and P. Claudin, Phys. Rev. Lett. **81**, 1841 (1998).
[5] D. Bi, J. Zhang, B. Chakraborty, and R. P. Behringer, Nature (London) **480**, 355 (2011).
[6] H. A. Vinutha and S. Sastry, Nat. Phys. **12**, 578 (2016).
[7] A. Y. Malkin, A. V. Mityukov, S. V. Kotomin, A. A. Shabeko, and V. G. Kulichikhin, J. Rheol. **64**, 469 (2020).
[8] N. Fernandez, R. Mani, D. Rinaldi, D. Kadau, M. Mosquet, H. Lombois-Burger, J. Cayer-Barrioz, H. J. Herrmann, N. D. Spencer, and L. Isa, Phys. Rev. Lett. **111**, 108301 (2013).
[9] R. Seto, R. Mari, J. F. Morris, and M. M. Denn, Phys. Rev. Lett. **111**, 218301 (2013).
[10] C. Heussinger, Phys. Rev. E **88**, 050201(R) (2013).
[11] N. Y. C. Lin, B. M. Guy, M. Hermes, C. Ness, J. Sun, W. C. K. Poon, and I. Cohen, Phys. Rev. Lett. **115**, 228304 (2015).
[12] C. Ness and J. Sun, Soft Matter **12**, 914 (2016).
[13] C. Clavaud, A. Bérut, B. Metzger, and Y. Forterre, Proc. Natl. Acad. Sci. U.S.A. **114**, 5147 (2017).
[14] A. Singh, C. Ness, R. Seto, J. J. de Pablo, and H. M. Jaeger, Phys. Rev. Lett. **124**, 248005 (2020).
[15] R. Mari, R. Seto, J. F. Morris, and M. M. Denn, J. Rheol. **58**, 1693 (2014).
[16] R. Seto, A. Singh, B. Chakraborty, M. M. Denn, and J. F. Morris, Granular Matter **21**, 82 (2019).
[17] M. Wyart and M. E. Cates, Phys. Rev. Lett. **112**, 098302 (2014).
[18] A. S. Baumgarten and K. Kamrin, Proc. Natl. Acad. Sci. U.S.A. **116**, 20828 (2019).
[19] P. R. Nott and J. F. Brady, J. Fluid Mech. **275**, 157 (1994).
[20] J. F. Morris and F. Boulay, J. Rheol. **43**, 1213 (1999).
[21] R. N. Chacko, R. Mari, M. E. Cates, and S. M. Fielding, Phys. Rev. Lett. **121**, 108003 (2018).
[22] H. Nakanishi, S.-I. Nagahiro, and N. Mitarai, Phys. Rev. E **85**, 011401 (2012).
[23] J. J. J. Gillissen, C. Ness, J. D. Peterson, H. J. Wilson, and M. E. Cates, Phys. Rev. Lett. **123**, 214504 (2019).
[24] S. Henkes, M. van Hecke, and W. van Saarloos, Europhys. Lett. **90**, 14003 (2010).
[25] S. Sarkar, D. Bi, J. Zhang, J. Ren, R. P. Behringer, and B. Chakraborty, Phys. Rev. E **93**, 042901 (2016).
[26] Y. Zhao, J. Barés, H. Zheng, J. E. S. Socolar, and R. P. Behringer, Phys. Rev. Lett. **123**, 158001 (2019).
[27] F. Gadala-Maria and A. Acrivos, J. Rheol. **24**, 799 (1980).
[28] N. Phan-Thien and N. Mai-Duy, *Understanding Viscoelasticity: An Introduction to Rheology* (Springer, Switzerland, 2017).
[29] P. Neff, B. Eidel, and R. J. Martin, Arch. Ration. Mech. Anal. **222**, 507 (2016).
[30] See Supplemental Material at http://link.aps.org/supplemental/10.1103/PhysRevLett.127.138001 for the derivation of Eq. (6), examples of identification of material parameters from experimental data; details on the dependence of simulation results on the meshing and on the values of the material parameters; and the full time evolution of pressure, flow, and elastic response, which includes Refs. [31–33].
[31] R. Seto, G. G. Giusteri, and A. Martiniello, J. Fluid Mech. **825**, R3 (2017).
[32] R. Seto and G. G. Giusteri, J. Fluid Mech. **857**, 200 (2018).
[33] C. Ness, R. Seto, and R. Mari, arXiv:2105.04162.